Particle-Support Interferences in Small-Angle X-Ray Scattering from Supported-Catalyst Materials

Tobias Binninger,[1,*] Marios Garganourakis,[2] Jun Han,[1] Alexandra Patru,[1] Emiliana Fabbri,[1] Olha Sereda,[2] Rüdiger Kötz,[1] Andreas Menzel,[1] and Thomas J. Schmidt[1,3]

[1]*Paul Scherrer Institut, CH-5232 Villigen PSI, Switzerland*
[2]*Centre Suisse d'Electronique et de Microtechnique SA, CH-2002 Neuchâtel, Switzerland*
[3]*ETH Zürich, Laboratory of Physical Chemistry, CH-8093 Zürich, Switzerland*

(Received 11 November 2014; revised manuscript received 13 January 2015; published 24 February 2015)

Small-angle x-ray scattering (SAXS) is a powerful technique for the investigation of catalyst materials at the nanoscale. We present results of an anomalous SAXS study on metal-oxide-supported platinum particles used as electrocatalysts for oxygen reduction. The scattering interferences between catalyst particles and support material are taken into account qualitatively and quantitatively by a mathematical model for the data-fitting procedure. Our results clearly demonstrate the fundamental importance of these catalyst-particle–support-material interferences in the analysis of SAXS data from supported catalysts.

DOI: 10.1103/PhysRevApplied.3.024012

I. INTRODUCTION

In the past two decades, small-angle x-ray scattering (SAXS) has become an established technique for the structural characterization at the nanoscale of catalyst particles supported on high-surface-area materials like carbon [1–8] and oxides [9–12]. From the scattering signal, information about catalyst-particle size, shape, and distribution can be derived. The advantage of SAXS over other complementary techniques like transmission electron microscopy (TEM) is that the scattered signal already contains the information averaged over millions of catalyst particles, whereas in TEM, sampling is comparably limited and highly time consuming. To be more specific, even for a synchrotron x-ray-beam diameter of the order of 100 μm, the beam easily probes 100 million catalyst nanoparticles within an acquisition time of seconds to minutes. Using TEM, a minimum of 1000 catalyst particles must be examined for achieving representative statistics. Due to shortcomings of TEM-data-analysis software, the determination of particle sizes is still preferentially done manually, one particle after the other, requiring hours to several days of analysis time. Furthermore, SAXS can be performed under *in situ* conditions, which allows one, e.g., to study the properties of fuel-cell catalysts during electrochemical testing [1–3,6–8]. Finally, for support materials containing high-Z elements, the support phase can have such a high TEM contrast that the supported nanoparticles become effectively invisible. In such a case, SAXS provides the only means to extract structural data about the catalyst particles at the nanoscale.

However, also for SAXS, the high-surface-area support complicates the analysis. First, the support material itself can strongly scatter to the small-angle region. And second, the scattering interference between catalyst particles and support additionally contributes to the total SAXS signal. The latter contribution is generally neglected in the analysis of SAXS data from supported catalysts. However, we show in the following that this interference effect can have a drastic influence on the SAXS curve, implying that the existing methods of SAXS analysis can strongly degrade the qualitative and quantitative findings. As a solution, we furthermore present a mathematical model which allows one to take this particle-support interference into account with high precision.

The full scattering signal contains contributions from both the catalyst nanoparticles and the support material and, if applicable, also from additional components like cell windows, etc. For the extraction of the pure scattering signal from the catalyst nanoparticles, there are two commonly used techniques: First, on laboratory x-ray diffractometers with fixed x-ray energy, the background scattering must be measured in a separate experiment with the bare support material. This signal can then be subtracted from the full supported-catalyst scattering intensities. However, the correct normalization of the two curves is often nontrivial. The second technique for the separation of catalyst-nanoparticle scattering from support scattering is anomalous SAXS (ASAXS). This technique can only be used at synchrotron SAXS beam lines because of the required tunability of the x-ray energy. The changes of the atomic form factors with energy around elemental absorption edges can be used to extract pure elemental scattering signals from SAXS curves recorded at different x-ray energies on the same sample.

For supported-catalyst nanoparticles, the full differential scattering cross section not only consists of the superposition of the individual scattering contributions of

*tobias.binninger@psi.ch

catalyst particles and support material, but it also contains the interference terms between catalyst particles and support phase,

$$\frac{d\sigma}{d\Omega}(\mathbf{q},E) = |f_p(E)|^2 n_p^2 S_{pp}(\mathbf{q}) + |f_s(E)|^2 n_s^2 S_{ss}(\mathbf{q}) + 2\mathrm{Re}[f_p(E) f_s^*(E)] n_p n_s S_{ps}(\mathbf{q}), \quad (1)$$

where p denotes the catalyst-particle phase and s denotes the support phase, and the differential cross section is understood in units of the Thomson differential cross section $r_0^2 = 7.95 \times 10^{-30}\ \mathrm{m}^2$ of a free electron in the forward direction [13]. Here, we adopt the notation as given in Ref. [14] in terms of the energy-dependent atomic form factors $f_i(E)$, the atomic (number) densities n_i, and the scattering-vector $\mathbf{q}$-dependent partial structure factors (PSFs) of phases $i, j \in \{p, s\}$,

$$S_{ij}(\mathbf{q}) = e^{-i\mathbf{q}\cdot(\mathbf{r_i}-\mathbf{r_j})} \int_V p_i(\mathbf{r}) e^{-i\mathbf{q}\cdot\mathbf{r}} d\mathbf{r} \int_V p_j(\mathbf{r}') e^{i\mathbf{q}\cdot\mathbf{r}'} d\mathbf{r}' = e^{-i\mathbf{q}\cdot(\mathbf{r_i}-\mathbf{r_j})} A_i(\mathbf{q}) A_j^*(\mathbf{q}), \quad (2)$$

where $p_i(\mathbf{r})$ is the spatial distribution function of phase i with value 1 for $\mathbf{r}$ inside phase i and value 0 everywhere else, and $A_i(\mathbf{q})$ is the Fourier transform thereof. The spatial distribution functions $p_{i,j}(\mathbf{r})$ are defined referring to the respective centers of origin $\mathbf{r}_{i,j}$ chosen for phases i, j. The exponential factor takes into account the overall phase shift for the case of differing centers of origin $\mathbf{r}_{i,j}$. In Eq. (1), we assume that the catalyst layer is statistically isotropic with the consequence that all PSFs are real quantities. Also, we do not take into account the void phase filling the pores of the catalyst layer. However, it can be easily shown that the void-phase scattering term $|f_v(E)|^2 n_v^2 S_{vv}(\mathbf{q})$ and the interference terms $2\mathrm{Re}[f_v(E) f_i^*(E)] n_v n_i S_{vi}(\mathbf{q})$ lead to an equation exactly analogous to Eq. (1) with the only difference that the atomic form factors f_i of catalyst particles and support material are replaced by the *effective* atomic form factors $\hat{f}_i = f_i - (n_v/n_i) f_v$. Therefore, in the following, we take the f_i to be the effective atomic form factors.

On the experimental side, the particle-support interferences $S_{ps}(\mathbf{q})$ are generally neglected in the published literature about SAXS and ASAXS on supported catalysts: Some authors assume the interference terms to be negligible in the relevant q range; others neglect them without any further comment. For the analysis of ASAXS data of supported-catalyst particles in Ref. [12], the theoretical work in Ref. [15] is used, where it is proven that the pure catalyst-particle scattering can be extracted by simply subtracting the SAXS curves recorded at two different energies close to the catalyst-particle elemental absorption edge. However, the derivation neglects the strong spatial correlations between catalyst particles and support material which give rise to exactly those particle-support interferences that we prove to have a significant influence on the SAXS curves. In particular, we show in the following how the commonly used *spherical particle* model can be extended to include the particle-support interferences.

II. THEORY

Assuming that the catalyst-particle phase p consists of only one single spherical particle of radius R, the Fourier transform results in the well-known structure factor,

$$A_p(q) = \frac{4}{3}\pi R^3 \left(3\frac{\sin(qR) - qR\cos(qR)}{(qR)^3}\right) = V(R) g(q,R)$$
$$\Rightarrow S_{pp}^{\mathrm{single}}(q) = |A_p(\mathbf{q})|^2 = V(R)^2 g(q,R)^2, \quad (3)$$

with the volume of the sphere $V(R)$ and the implicit definition of the function $g(q,R)$, which has the property $\lim_{q\to 0} g(q,R) = 1$. The result only depends on the magnitude q of the scattering vector. This structure factor is generally used together with a certain distribution function for the particle radius R to fit the experimentally extracted catalyst-particle scattering data. This experimental extraction procedure consists of subtracting the total differential cross sections measured at two different energies E_1 and E_2 close to the catalyst-particle elemental absorption edge. In this energy range, the catalyst-particle atomic form factor substantially varies in energy, and the support-material atomic form factor f_s can in most cases be assumed to be energy independent. Therefore, the pure support-material scattering $|f_s|^2 n_s^2 S_{ss}(\mathbf{q})$ cancels, and, neglecting the interference term $S_{ps}(\mathbf{q})$, the difference is equal to $[|f_p(E_1)|^2 - |f_p(E_2)|^2] n_p^2 S_{pp}(\mathbf{q})$, which yields $S_{pp}(\mathbf{q})$ after dividing by the scattering contrast $[|f_p(E_1)|^2 - |f_p(E_2)|^2] n_p^2$. However, if we take the interference term into account, then this procedure yields the true ASAXS-subtracted signal,

$$\frac{\frac{d\sigma}{d\Omega}(\mathbf{q},E_1) - \frac{d\sigma}{d\Omega}(\mathbf{q},E_2)}{[|f_p(E_1)|^2 - |f_p(E_2)|^2] n_p^2} = S_{pp}(\mathbf{q}) + \frac{2\mathrm{Re}\{[f_p(E_1) - f_p(E_2)] f_s^*\} n_p n_s}{[|f_p(E_1)|^2 - |f_p(E_2)|^2] n_p^2} S_{ps}(\mathbf{q}) \approx S_{pp}(\mathbf{q}) + \frac{f_s n_s}{\bar{f}_p n_p} S_{ps}(\mathbf{q}) = S_{pp}(\mathbf{q}) + \alpha S_{ps}(\mathbf{q}), \quad (4)$$

where $\bar{f}_p$ is the average of the catalyst-particle atomic form factors $f_p(E_1)$ and $f_p(E_2)$ at the two energies, and α is referred to as the support-catalyst scattering ratio in the following. The final approximation directly follows if we neglect the imaginary parts of the atomic form factors f_p and f_s. In this way, it becomes evident that the relative

strength of the interference term compared to the pure catalyst-particle scattering term is approximately equal to the ratio of the support atomic form factor (times support atomic density) over the average catalyst-particle atomic form factor (times catalyst-particle atomic density). For certain systems like light-metal nanoparticles on a high-Z metal-oxide support, this ratio can become larger than 1. Therefore, the particle-support interference cannot be neglected in the ASAXS-subtracted signal *a priori*.

In order to understand the behavior of $S_{ps}(\mathbf{q})$ in more detail, we calculate its analytical form for the model of a single spherical catalyst particle with radius R_p sitting on a single spherical support particle with radius $R_s > R_p$, as shown in the inset in Fig. 1. We assume a point contact between catalyst particle and support particle, so that $|\mathbf{r_p} - \mathbf{r_s}| = R_p + R_s$. Then, the interference term $S_{ps}(\mathbf{q})$ can be directly evaluated according to Eq. (2) to yield

$$S_{ps}^{\text{single}}(\mathbf{q}) = e^{-iq(R_p+R_s)\cos\theta} \times V(R_p)V(R_s)g(q,R_p)g(q,R_s), \quad (5)$$

where we rewrite the scalar product $\mathbf{q}\cdot(\mathbf{r_p} - \mathbf{r_s}) = q(R_p + R_s)\cos\theta$. In the catalyst layer, the relative orientations of the catalyst particles and the respective supporting particles are completely random, so that the sum over all catalyst particles introduces an average $\langle\ldots\rangle_{\theta,\phi}$ over the polar angle θ and the azimuthal angle ϕ between $\mathbf{q}$ and $(\mathbf{r_p} - \mathbf{r_s})$. This average solely affects the exponential factor,

$$\langle e^{-iq(R_p+R_s)\cos\theta}\rangle_{\theta,\phi} = \frac{\sin[q(R_p+R_s)]}{q(R_p+R_s)}, \quad (6)$$

with the property $\lim_{q\to 0}\ldots = 1$. The structure factor $\langle S_{ps}^{\text{single}}(q)\rangle_{\theta,\phi}$ then depends only on the magnitude q of the scattering vector. Finally, the polydispersities both in the catalyst-particle size and the support-particle size must be taken into account in the total PSFs describing the full catalyst layer. These polydispersities are expressed in terms of the catalyst-particle size distribution $P_p(R_p)$ and the support-particle size distribution $P_s(R_s)$, so that the total PSFs read

$$S_{pp}(q) = N_p \int_0^\infty [P_p(R_p)V(R_p)^2 g(q,R_p)^2]dR_p, \quad (7)$$

$$S_{ps}(q) = N_p \iint_0^\infty \left\{ P_p(R_p)P_s(R_s)V(R_p)V(R_s) \times g(q,R_p)g(q,R_s)\frac{\sin[q(R_p+R_s)]}{q(R_p+R_s)}\right\} dR_p dR_s, \quad (8)$$

where N_p is the total number of catalyst particles irradiated by the x-ray beam. In Fig. 1, the particle scattering S_{pp}, the interference term S_{ps}, and the ASAXS-subtracted signal $S_{pp} + \alpha S_{ps}$ for $\alpha = 1$ are plotted on a double-logarithmic scale. In this case, the particle size distributions P_p and P_s are taken to be commonly used log-normal distributions,

$$P_i(R_i) = \frac{1}{\sqrt{2\pi}R_i\sigma_i} e^{-\frac{[\ln(R_i/\mu_i)]^2}{2\sigma_i^2}}. \quad (9)$$

The interference PSF $S_{ps}(q)$ has negative values at larger q (cf. the Supplemental Material [16]), and a positive limiting value of $N_p\langle V_p\rangle\langle V_s\rangle$ for $q \to 0$. This value is larger than the limiting value $\lim_{q\to 0} S_{pp}(q) = N_p\langle V_p^2\rangle$, so that S_{ps} dominates at small q in the ASAXS-subtracted signal, whereas S_{pp} generally dominates at larger q. In the transition region between these two q ranges, the entire signal after ASAXS subtraction, Eq. (4), can become negative, depending on the support-catalyst scattering ratio α and the relative size difference between catalyst and support particles. Such a region of negative values in an experimental ASAXS-subtracted signal is clear evidence of the catalyst-particle–support-material interference, because the pure particle scattering $S_{pp} = |A_p|^2$ is strictly positive.

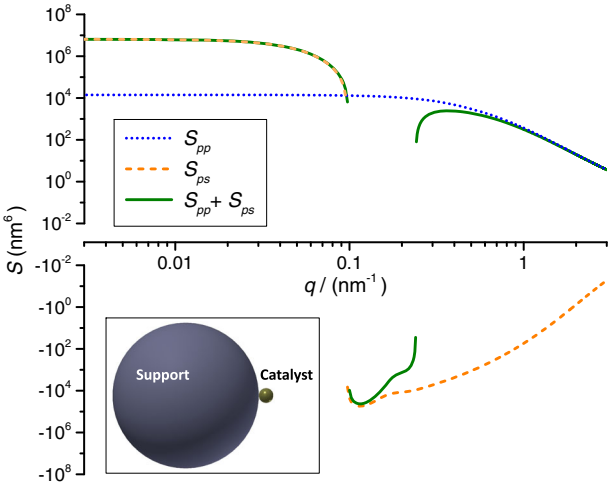

FIG. 1. The catalyst-particle PSF $S_{pp}(q)$ (dark-blue dotted line), Eq. (7), the particle-support interference PSF $S_{ps}(q)$ (light-orange dashed line), Eq. (8), and the sum of both (solid line), which is equal to the ASAXS-subtracted signal for $\alpha = 1$. The inverted second logarithmic y axis allows regions of negative values of the PSFs to be displayed. The model of spherical catalyst particles supported on spherical support particles shown in the inset is used. The catalyst and support-particle size distributions are taken to be log-normal distributions, Eq. (9), with parameters $\mu_p = 1.5$ nm, $\sigma_p = 0.5$, $\mu_s = 30$ nm, and $\sigma_s = 0.25$.

III. EXPERIMENT

Anomalous SAXS experiments are performed at the cSAXS beam line X12SA at the Swiss Light Source (SLS)

synchrotron at Paul Scherrer Institut, Switzerland. The SAXS curves are recorded with a Pilatus 2M detector [17], which is placed at the end of a 2.1-m-long evacuated flight tube. The scattering curves are corrected for sample absorption, isotropic background scattering, and photon-detection efficiency and then transformed to differential cross sections per area by normalization with respect to the incident photon current. The absolute calibration of the photodiode measuring the transmitted photon current is done with a glassy carbon standard [18]. The investigated catalyst consists of platinum nanoparticles supported on iridium-titanium oxide (Pt/IrO_2-TiO_2) and is provided by Umicore AG & Co. KG [19]. The Pt content is 8.8 wt %, and the support oxide consists of two separate phases of IrO_2 (≈66 mol%) and TiO_2 (≈34 mol%). This material serves as a benchmark for the research on stable metal-oxide-supported platinum catalysts for the oxygen electrode of polymer electrolyte fuel cells (PEFC) [20]. The SAXS measurements are conducted *in situ* during electrochemical testing of the catalyst material in aqueous 0.1*M* $HClO_4$ electrolyte. Anomalous SAXS is used to filter out the Pt scattering from the overall signal. The Ir-containing support oxide added a further complication to the anomalous SAXS analysis because the energy dependence of the Ir atomic form factor could not be neglected in the experimental energy range of the Pt L_{III}-absorption edge ($E_{\mathrm{Pt},L_{\mathrm{III}}} = 11.56$ keV [21]). Additionally, the *in situ* flow-cell setup contained a thin gold layer for the electrical contact, and the energy dependence of the Au atomic form factor also has to be taken into account. Therefore, SAXS curves are recorded at the four energies ($E_1 = 11.20$ keV, $E_2 = 11.45$ keV, $E_3 = 11.55$ keV, and $E_4 = 11.70$ keV) and the analysis is adjusted accordingly, as described in the Supplemental Material [16]. Nevertheless, the result of this analysis is analogous to Eq. (4), $S_{pp}(q) + \alpha S_{ps}(q)$, with the difference of a more complicated expression for the prefactor α of the interference term S_{ps}. The energy-dependent values of the elemental atomic form factors used in the ASAXS analysis are taken from Ref. [22].

The experimental Pt signal after ASAXS analysis is plotted in Fig. 2. The statistical data error estimated from Poisson photon-counting statistics is of the same magnitude as the obvious fluctuations in the plotted data. The data show a region of negative values in the intermediate q range, which is a clear signature of the particle-support interference as described above. Also shown is the fit of the data with the function $S_{pp}(q) + \alpha S_{ps}(q)$, with $S_{pp}(q)$ and $S_{ps}(q)$ by Eqs. (7) and (8). The particle size distributions $P_p(R_p)$ and $P_s(R_s)$ are both chosen to be of log-normal type, Eq. (9). This model incorporating the particle-support interference has the six free fitting parameters (μ_p, σ_p, μ_s, σ_s, α, and N_p) and the respective fit is in very good agreement with the experimental data. The fit yields the Pt-particle size distribution $P_p(R_p)$ shown in the inset in Fig. 2 with average Pt-particle radius $\langle R_p \rangle = 1.0$ nm and standard deviation $s_{R_p} = 0.15$ nm. The effective average support-particle radius is found to be $\langle R_s \rangle = 12$ nm. The fitted value of $\alpha = 0.72$ is slightly larger than the value of 0.54 estimated from the respective atomic form factors as described in the Supplemental Material [16]. This difference might result first from an uncertainty of the fitted value due a decrease of the experimental-data precision at low q, and second from an imprecision of the theoretically estimated value due to the assumption that the Pt particles are homogeneously distributed with equal properties over both the IrO_2 and the TiO_2 partial phases of the support. Also shown in Fig. 2 is the pure Pt PSF $S_{pp}(q)$ resulting from the Pt-particle size distribution as determined from the fit with the full model. It is evident that it would be impossible to obtain this correct Pt PSF if the data were fitted only with the function $S_{pp}(q)$ from Eq. (8).

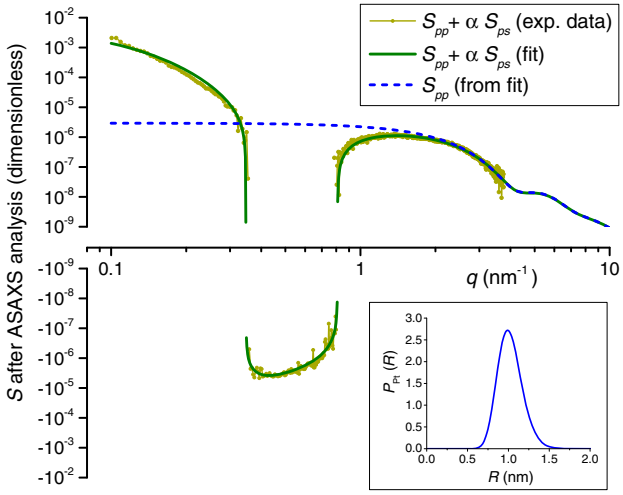

FIG. 2. Experimental ASAXS-subtracted data from Pt/IrO_2-TiO_2 catalyst (dots with line). The data are fitted with the model for $S_{pp} + \alpha S_{ps}$ with log-normal catalyst-particle and support-particle size distributions (solid line). Also shown is the pure Pt-particle PSF S_{pp} resulting from the fitted particle size distribution (dashed line). The inset shows the log-normal Pt-particle (radius) size distribution determined from the fit to the experimental data.

IV. DISCUSSION

Even for a standard platinum-on-carbon (Pt/C) catalyst, the support-catalyst scattering ratio is $\alpha \approx f_C n_C/(f_{Pt} n_{Pt}) \approx 0.2$ (for graphite carbon), so that the interference can be expected to be visible in the SAXS curve. In such a case of smaller α, the ASAXS-subtracted signal can lose the region of negative values and then resemble a sole catalyst-particle PSF $S_{pp}(q)$ for a bimodal catalyst-particle size distribution. Thus, the particle-support interference easily can be misinterpreted in this way if not correctly taken into account.

A refit of the published Pt/C data from Ref. [3] with our model including the particle-support interference and a unimodal Pt-particle size distribution is presented in the Supplemental Material [16].

Another approach to deal with the particle-support interference is to separate it experimentally instead of incorporating it into a theoretical fitting model. In principle, this separation is possible because the energy dependence of the prefactor of the interference term in Eq. (1) is linearly independent of the other prefactors. So, by recording SAXS curves at sufficiently many x-ray energies, the system of equations can be inverted to yield S_{pp}, S_{ps}, and S_{ss} individually. This experimental strategy has been proposed for the general case of binary materials [23]. It has been applied in the ASAXS analysis of alloys [24] and also in a recent study in the analysis of ASAXS data from carbon-supported metal-alloy nanoparticles [8]. To our knowledge, Ref. [8] is the only published SAXS study on supported-catalyst particles where the authors tried to fully separate the individual PSFs experimentally. However, the authors did not provide the respective results concerning the separated PSFs. The general reason for the lack of experimental data might be the fact that this experimental strategy requires extremely high data precision because the invertibility of the respective system of equations, Eq. (1), for different energies is difficult to achieve within experimental errors. Therefore, our proposed theoretical approach to incorporate the particle-support interference into the fitting function for the (A)SAXS data appears to be much more feasible.

V. CONCLUSION

The strong spatial correlations between catalyst particles and support material lead to interference effects in SAXS, which have to be taken into account. We develop a model incorporating the particle-support interference that allows fitting the experimental data after applying the usual ASAXS analysis. The model is proven to be successful in the analysis of ASAXS data of a Pt/IrO_2-TiO_2 PEFC catalyst. It is also shown that the conventional ASAXS analysis neglecting the particle-support interference fails to provide a physically meaningful fit to the data. Therefore, we strongly believe that these interferences must be taken into account in the analysis of any SAXS experiment on supported-catalyst materials. It should be noted that this conclusion also applies to SAXS data obtained on laboratory diffractometers, where the support scattering is determined in a separate experiment and subtracted from the full catalyst signal. Also here, the particle-support interferences remain present in the difference scattering curve. Therefore, our findings enable a drastic improvement of the characterization of supported-catalyst materials by (A)SAXS using both synchrotron facilities and laboratory x-ray diffractometers.

ACKNOWLEDGMENTS

This work was supported by Competence Center for Energy and Mobility (CCEM) Switzerland and Umicore AG & Co. KG within the project DuraCat. We gratefully thank Michael Horisberger for the help in connection with the electrode preparation. We acknowledge the Paul Scherrer Institut, Villigen, Switzerland, for provision of synchrotron radiation beam time at the cSAXS beam line of the SLS and we would like to thank Dr. Ana Diaz for assistance.

[1] H. G. Haubold, X. H. Wang, H. Jungbluth, G. Goerigk, and W. Schilling, *In situ* anomalous small-angle x-ray scattering and x-ray absorption near-edge structure investigation of catalyst structures and reactions, J. Mol. Struct. **383**, 283 (1996).

[2] H.-G. Haubold, X. H. Wang, G. Goerigk, and W. Schilling, *In situ* anomalous small-angle x-ray scattering investigation of carbon-supported electrocatalysts, J. Appl. Crystallogr. **30**, 653 (1997).

[3] H. G. Haubold, P. Hiller, H. Jungbluth, and T. Vad, Characterization of electrocatalysts by *in situ* SAXS and XAS investigations, Jpn. J. Appl. Phys. **38**, 36 (1999).

[4] A. Benedetti, L. Bertoldo, P. Canton, G. Goerigk, F. Pinna, P. Riello, and S. Polizzi, ASAXS study of Au, Pd and Pd-Au catalysts supported on active carbon, Catal. Today **49**, 485 (1999).

[5] C. Yu, S. Koh, J. E. Leisch, M. F. Toney, and P. Strasser, Size and composition distribution dynamics of alloy nanoparticle electrocatalysts probed by anomalous small angle x-ray scattering (ASAXS), Faraday Discuss. Chem. Soc. **140**, 283 (2008).

[6] M. C. Smith, J. A. Gilbert, J. R. Mawdsley, S. Seifert, and D. J. Myers, *In situ* small-angle x-ray scattering observation of Pt catalyst particle growth during potential cycling, J. Am. Chem. Soc. **130**, 8112 (2008).

[7] J. A. Gilbert, N. N. Kariuki, R. Subbaraman, A. J. Kropf, M. C. Smith, E. F. Holby, D. Morgan, and D. J. Myers, *In situ* anomalous small-angle x-ray scattering studies of platinum nanoparticle fuel cell electrocatalyst degradation, J. Am. Chem. Soc. **134**, 14823 (2012).

[8] X. Tuaev, S. Rudi, V. Petkov, A. Hoell, and P. Strasser, *In situ* study of atomic structure transformations of Pt-Ni nanoparticle catalysts during electrochemical potential cycling, ACS Nano **7**, 5666 (2013).

[9] F. Berg Rasmussen, A. M. Molenbroek, B. S. Clausen, and R. Feidenhans, Particle size distribution of an Ni/SiO_2 catalyst determined by ASAXS, J. Catal. **190**, 205 (2000).

[10] S. Polizzi, P. Riello, A. Balerna, and A. Benedetti, Nanostructure of Pd/SiO_2 supported catalysts, Phys. Chem. Chem. Phys. **3**, 4614 (2001).

[11] S. Polizzi, P. Riello, G. Goerigk, and A. Benedetti, Quantitative investigations of supported metal catalysts by ASAXS, J. Synchrotron Radiat. **9**, 65 (2002).

[12] H. Brumberger, D. Hagrman, J. Goodisman, and K. D. Finkelstein, *In situ* anomalous small-angle x-ray scattering

from metal particles in supported-metal catalysts. II. Results, J. Appl. Crystallogr. **38**, 324 (2005).

[13] J. Als-Nielsen and D. McMorrow, *Elements of Modern X-Ray Physics*, 2nd ed. (Wiley, Chichester, 2011).

[14] D. Tatchev, Structure analysis of multiphase systems by anomalous small-angle x-ray scattering, Philos. Mag. **88**, 1751 (2008).

[15] H. Brumberger, D. Hagrman, J. Goodisman, and K. D. Finkelstein, *In situ* anomalous small-angle x-ray scattering from metal particles in supported-metal catalysts. I. Theory, J. Appl. Crystallogr. **38**, 147 (2005).

[16] See Supplemental Material at http://link.aps.org/supplemental/10.1103/PhysRevApplied.3.024012 for a mathematical discussion of the interference PSF $S_{ps}(\mathbf{q})$, a detailed description of the ASAXS analysis procedure for the Pt/IrO_2-TiO_2 catalyst, and a refit of published Pt/C ASAXS data with the model, including the particle-support interference.

[17] B. Henrich, A. Bergamaschi, C. Broennimann, R. Dinapoli, E. F. Eikenberry, I. Johnson, M. Kobas, P. Kraft, A. Mozzanica, and B. Schmitt, Pilatus: A single photon counting pixel detector for x-ray applications, Nucl. Instrum. Methods Phys. Res., Sect. A **607**, 247 (2009).

[18] F. Zhang, J. Ilavsky, G. G. Long, J. P. G. Quintana, A. J. Allen, and P. R. Jemian, Glassy carbon as an absolute intensity calibration standard for small-angle scattering, Metall. Mater. Trans. A **41**, 1151 (2010).

[19] J. P. Suchsland, B. Klose-Schubert, D. Herein, T. Martin, C. Eickes, and M. Lennartz, The potential of non carbon based catalysts for automotive fuel cells, ECS Trans. **50**, 1659 (2013).

[20] T. Binninger, E. Fabbri, R. Kötz, and T. J. Schmidt, Iridium-titanium oxide as support for Pt catalyst in PEFC cathodes, ECS Trans. **58**, 1835 (2013).

[21] S. Kraft, J. Stümpel, P. Becker, and U. Kuetgens, High resolution x-ray absorption spectroscopy with absolute energy calibration for the determination of absorption edge energies, Rev. Sci. Instrum. **67**, 681 (1996).

[22] B. L. Henke, E. M. Gullikson, and J. C. Davis, http://henke.lbl.gov/optical_constants, accessed 2014-06-10.

[23] H. B. Stuhrmann, Resonance scattering in macromolecular structure research, Adv. Polym. Sci. **67**, 123 (1985).

[24] A. Hoell, D. Tatchev, S. Haas, J. Haug, and P. Boesecke, On the determination of partial structure functions in small-angle scattering exemplified by $Al_{89}Ni_6La_5$ alloy, J. Appl. Crystallogr. **42**, 323 (2009).